catalysts

MDPI

Communication

Enhancement Photocatalytic Activity of the Heterojunction of Two-Dimensional Hybrid Semiconductors ZnO/V_2O_5

Juan Aliaga [1], Nasla Cifuentes [1], Guillermo González [3,4,*], Clivia Sotomayor-Torres [5,6] and Eglantina Benavente [1,2,*]

1 Departamento de Química, Facultad de Ciencias Naturales, Universidad Tecnológica Metropolitana, Matemáticas y Medio Ambiente, P.O. Box 9845, Santiago, Chile; jaliaga@utem.cl (J.A.); nas.cifuentes@gmail.com (N.C.)
2 Programa Institucional de Fomento a la I+D+i, Universidad Tecnológica Metropolitana, Ignacio Valdivieso 2409, P.O. Box 8940577, San Joaquín, Santiago, Chile
3 Departamento de Química, Facultad de Ciencia, Universidad de Chile, P.O. Box 653, Santiago, Chile
4 Center for the Development of Nanoscience and Nanotechnology, CEDENNA, Av. Ecuador 3493, Santiago, Chile
5 Catalan Institute of Nanoscience and Nanotechnology (ICN2), CSIC and BIST, Campus UAB Bellaterra, 08193 Barcelona, Spain; clivia.sotomayor@icn2.cat
6 ICREA, Pg. Lluís Companys 23, 08010 Barcelona, Spain
* Correspondence: ggonzale@uchile.cl (G.G.); ebenaven@utem.cl (E.B.); Tel.: +56-22-978-7404 (G.G.); +56-22-787-7109 (E.B.)

Received: 30 July 2018; Accepted: 27 August 2018; Published: 4 September 2018

Abstract: In this work, we report the fabrication of the new heterojunction of two 2D hybrid layered semiconductors—ZnO (stearic acid)/V_2O_5 (hexadecylamine)—and its behavior in the degradation of aqueous methylene blue under visible light irradiation. The optimal photocatalyst efficiency, reached at a ZnO (stearic acid)/V_2O_5 (hexadecylamine) ratio of 1:0.25, results in being six times higher than that of pristine zinc oxide. Reusability test shows that after three photocatalysis cycles, no significant changes in either the dye degradation efficiency loss, nor the photocatalyst structure, occur. Visible light photocatalytic performance observed indicates there is synergetic effect between both 2D nanocomposites used in the heterojunction. The visible light absorption enhancement promoted by the narrower bandgap V_2O_5 based components; an increased photo generated charge separation favored by extensive interface area; and abundance of hydrophobic sites for dye adsorption appear as probable causes of the improved photocatalytic efficiency in this hybrid semiconductors heterojunction. Estimated band-edge positions for both conduction and valence band of semiconductors, together with experiments using specific radical scavengers, allow a plausible photodegradation mechanism.

Keywords: photocatalysis; heterojunction; two-dimensional semiconductor; ZnO; V_2O_5; Methylene blue degradation

1. Introduction

The use of solar energy is increasingly needed to address many of the growing energy and environmental problems facing humanity. Processes like the production of clean fuels from abundant natural resources or the degradation of pollutants based on sunlight-driven reactions, catalyzed by nanostructured semiconducting metal oxides, have received much attention during the last decades [1,2]. These are heterogeneous processes where the role of the photocatalyst is like that of the

electrodes in electrolysis in the sense of promoting, separately but simultaneously, a redox reactions pair with given substrates adsorbed on its surface. The conversion of radiation energy into chemical energy mainly depends on both, the ability of the semiconductor for creating effective redox centers on its surface and the tendency of the substrate to be adsorbed nears these sites. The photoinduced creation of active redox sites starts with the excitation of electrons from the valence band of the semiconductor to the conduction one, by the absorption of light with energy equal to or greater than its band-gap generating electron-hole pairs (e^-/h^+). After the separation of these charge pairs, mediated by internal or external electric fields, electrons and holes migrate to spatially separated places at the interface between the particle with its environment, where they can respectively reduce or oxidize suitable substrates [3,4].

The use of wide band, high valence metal oxides, such as TiO_2 and more recently ZnO, as photocatalysts have been extensively studied. The electronic structure of these semiconductors, particularly the position of their valence band edge (about 3.0 eV vs. NHE), provides interesting photochemical activity and high resistance to photocorrosion in water solutions; this, together with their generally non-toxicity and low cost, make them promissory for large-scale environmental remediation applications [5,6]. However, their photocatalytic efficiency and thus their large-scale applications, is affected by some of their intrinsic properties. Among them, a narrow absorption window that excludes much of the solar spectrum; high recombination rates of light-induced charges leading to poor quantum yields; and relatively high hydrophilic surfaces unfavorable for the adsorption of non-polar substrates [7]. Many efforts have been invested in solving these hindrances. Although most reports on this subject concern TiO_2, during the last years ZnO a n-type semiconductor with direct band gap (3.37 eV) and high exciton binding energy (60 meV), has received increasing attention [8,9]. The role of the morphology of ZnO nanostructures on its photocatalytic performance in the decomposition of organic molecules is being intensively studied [10,11]. In general, anisotropic micro/nanostructures are more efficient because, together with promoting charge carrier generation rate (nanoscale), they allow a higher mean-path-length for the photoinduced charges. This, among others, reduces charge-carriers' recombination, promotes effective charge separation and makes more facile the migration of charge carriers to their reaction sites. Similar effects have been attained by loading noble metals such as Au, Ag, Pd and Pt as co-catalysts [12–14] and by the formation of ZnO heterojunctions with other semiconductors like TiO_2, $BiVO_4$, Ag_2O or Cu_2O [14–18]. Numerous attempts to extend the light absorption window of ZnO —naturally centered in the ultraviolet— towards lower energies have been also reported [19]. ZnO sensitization by heterojunction with a relatively minor amount of a second lower band gap semiconductor like CdS or WO_3 [20,21] has been demonstrated to effectively improve its photocatalytic activity under visible light. In these systems, the main absorber is the secondary semiconductor while the role of ZnO is principally limited to the charge curriers transport. That notwithstanding, some interesting approaches to directly improve ZnO visible-light absorption have been also attempted; namely by creating electronic levels within the ZnO band gap, by metal or non-metal doping, or surface modification via organic materials grafting [22–25]. Most attempts to improve the photocatalysis of organic contaminants by optimizing the adsorption of the substrates upon the photocatalyst mainly concern the increment of its specific surface area, so the utilization of 2D layered materials that have larger specific surface areas—a great number of active sites on the surface and superior electron mobility that facilitates the transfer and separation of photogenerated electrons and holes—is a good strategy for constructing effective photocatalyst [26,27]. Approach considering additives to increase the hydrophobicity of the semiconductor surface, like the use of surfactants reported for TiO_2 are in general scarce for ZnO [25,28–32]. In this direction, we recently developed laminar hybrid 2D ZnO-organic nanocomposites in which the surfactant, grafted to the inorganic matrix, significantly improves the photocatalytic process [33]. The sensitization of ZnO with V_2O_5 species has been previously informed; for example, Yin et al. reported enhanced photocatalytic degradation of methylene blue (MB) in V_2O_5/ZnO heteronanorods [34], Zou et al. reported the decomposition of chlorophenol asisted by ZnO/V_2O_5 core-shell nanostructures [35],

and Aslam et al. reported the decomposition of nitrophenol with bare ZnO/V_2O_5 mixtures [36]. The capability of V_2O_5 to sensitize the ZnO nanocomposite makes the system a very attractive and new material for studied of heterogeneous photocatalysis.

In this work, we evaluated the photocatalytic activity of the organic-inorganic laminar ZnO (stearic acid) with a band gap (Eg) of 3.28 eV, combined with organic-inorganic hybrid V_2O_5 (hexadecylamine), (Eg = 3.28) in the degradation of aqueous methylene blue solution in visible light. In addition, we have realized various combinations with V_2O_5 and V_2O_5-xerogel to investigate the photocatalytic activity. The blend of both organic-inorganic hybrid semiconductors 2D/2D produces the expected synergy improving the degradation of the dye selected as organic contaminant model. Furthermore, tentative mechanism was also discussed based on the active species trapping experiments and estimated band edge positions.

2. Results and Discussion

The XRD pattern of synthesized nanocomposites are shown in Figure 1. The lamellar nature of ZnO (stearic acid) (ZnO(SA)), shown in Figure 1a, and V_2O_5 (hexadecylamine) (V_2O_5(HDA)), shown in Figure 1b, which were constituted of single nanosheets of semiconductor sandwiched between self-assembled surfactants, is confirmed by the X-ray diffraction patterns. These display low angle reflections, characteristic of well-ordered laminar arrangements 2D, according to the positions of the 00l reflections in the diffraction pattern. The interlayer distances along the c-axis correspond to the first peak in the low angle XRD pattern, which correlate well with the molecular lengths of corresponding carboxylic acid and alkylamine, previously reported [37,38]. In Figure 1a also shows the reflections that indicate the inorganic moiety corresponding to ZnO single phase with the wurtzite structure (JCPDS 36-1451). Figure 1c shows the XRD patterns of heterojunction ZnO(SA)/V_2O_5(HDA); two types of phases were detected, a phase well defined of ZnO(SA) and a 001 plane to V_2O_5(HDA), reveal the formation of layered structure with both composites. In this XRD pattern, no other possible impurities were detected which do suggest that nanocomposites ZnO(SA) and V_2O_5(HDA) remains unaltered.

The chemical states of the ZnO(SA)/V_2O_5(HDA) composite were investigated by X-ray photoelectron spectra (XPS) as shown in Figure 2. The XPS survey spectra (Figure S1) indicate the presence of Zn, V, O and C in the surface of the composite. The deconvolution of the high-resolution spectra for Zn 2p, V 2p and O 1s is shown in the Figure 2a–c. The binding energies for the Zn $2p_{3/2}$ and $2p_{1/2}$ core levels at 1021.6 eV and 1044.6 eV respectively in Figure 2a, indicates the presence of ZnO in the composite. The Figure 2b, show the V $2p_{3/2}$ spectrum of the composite, with two components centered at 516.8 eV and 515.5 eV, corresponding to the binding energies for the V^{5+} and V^{4+} species, in agreement with the presence of V_2O_5 and VO_2 [39]. The O 1s spectrum (Figure 2c) contains two peaks, at 530 eV and 531 eV with characteristic binding energies for O-oxidation state and the peak at 531–532 eV has been assigned to the oxygen of surfactants of the composite [40].

Scanning electron microscopy (SEM) were performed to investigate the morphology and microstructures of nanocomposite samples. The morphology of nanocomposites is illustrated in the micrographics in Figure 3. The SEM image shows in Figure 3a,b the layered nature of ZnO(SA) and V_2O_5(HDA) while its microstructured surface, with multi-layer laminas. Figure 3c presents the SEM images of the representative ZnO(SA)/V_2O_5(HDA) heterojunction and EDX patterns of confirm the presence of all constituent elements of the heterojunction. No other remarkable impurities were observed. In Figure S2 SEM images of ZnO(SA)/V_2O_5(HDA) and element mappings were further performed, and it can be seen clearly that Zn and V are evenly distributed, indicating the formation of hybrid nanostructure.

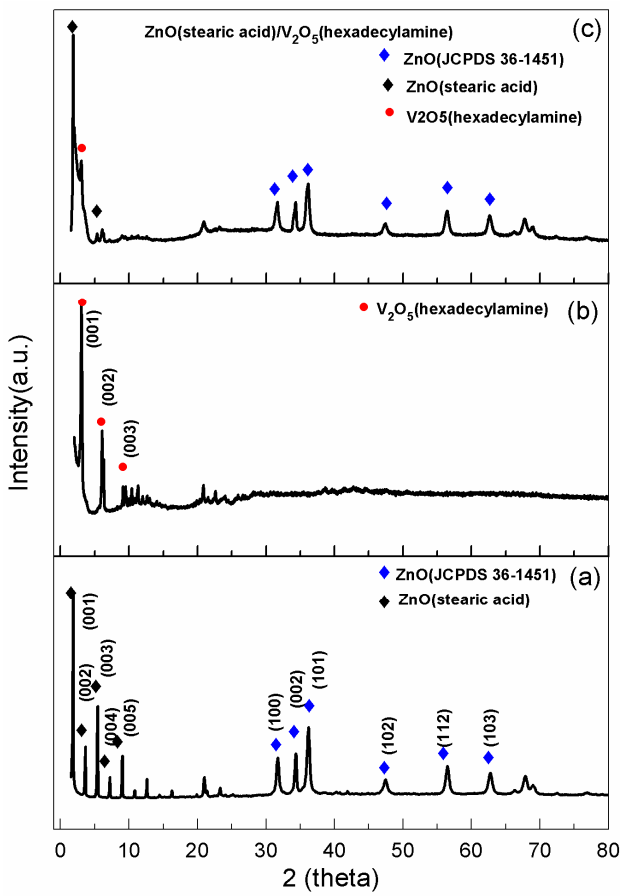

Figure 1. (**a**) XRD pattern of ZnO(SA); (**b**) XRD pattern of V_2O_5(HDA); and (**c**) XRD pattern of nanocomposite heterojunction ZnO(SA)/V_2O_5(HDA).

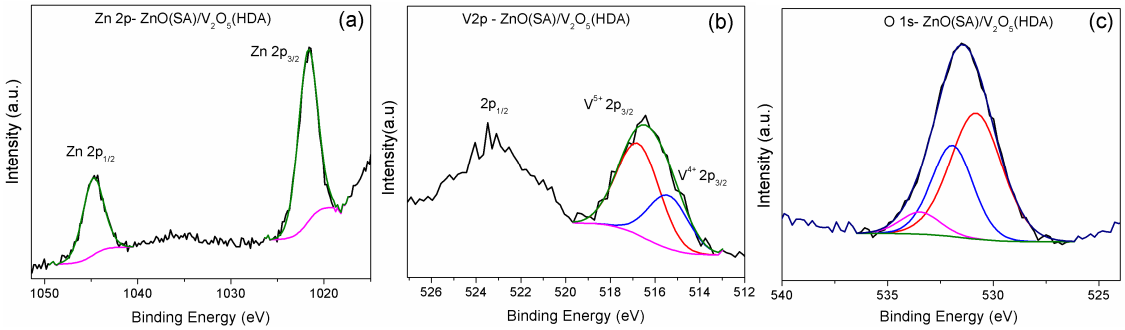

Figure 2. XPS spectra of core level (**a**) Zn2p, (**b**) V2p and (**c**) O1s.

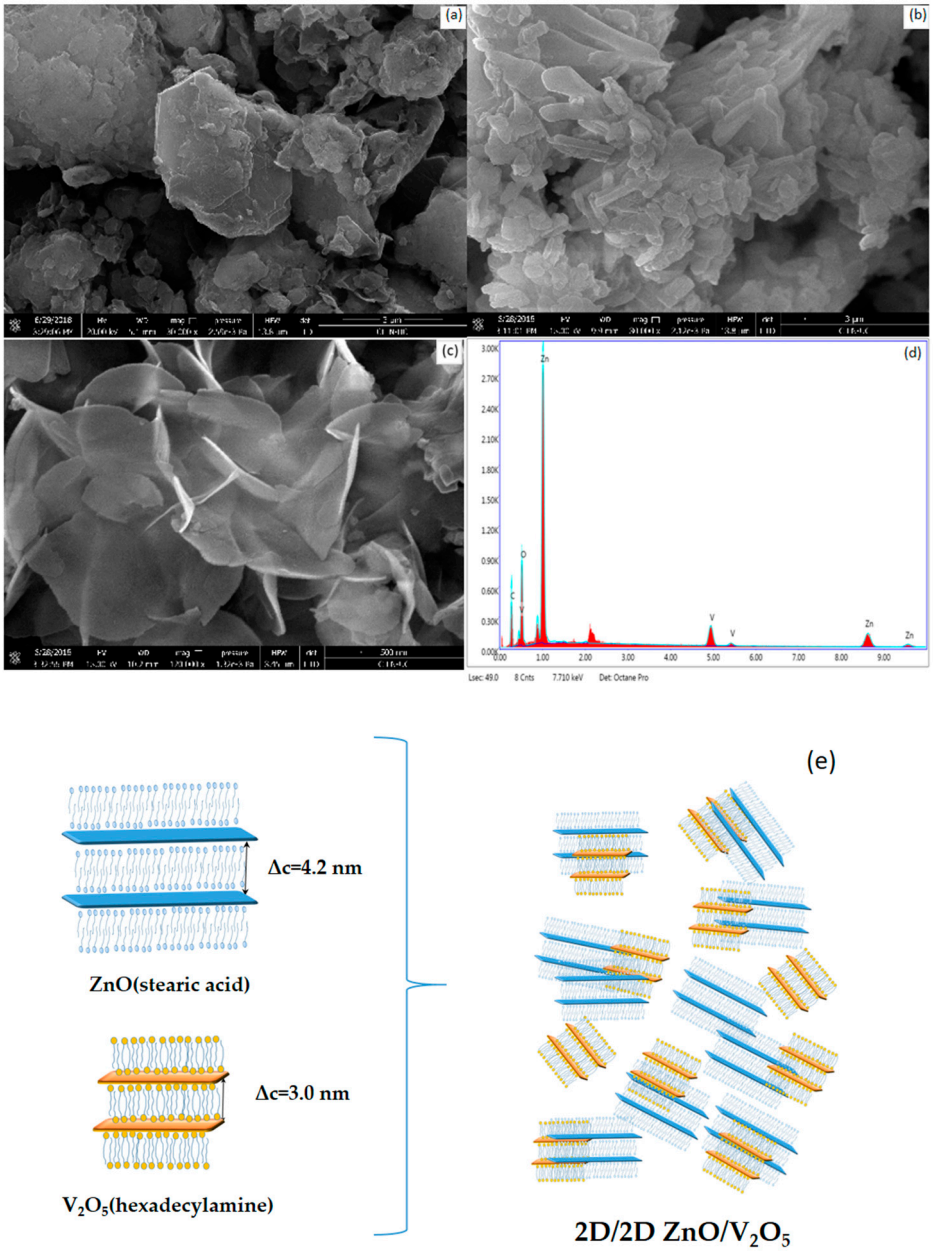

Figure 3. (**a**) SEM micrographs ZnO(SA); (**b**) SEM micrographs V_2O_5(HDA); (**c**) SEM micrographs ZnO(SA)/V_2O_5(HDA); (**d**) EDX pattern and (**e**) Schematic representation 2D/2D heterojunction.

The UV–visible diffuse reflectance was measured for ZnO(SA), V_2O_5(HDA) and ZnO(SA)/V_2O_5(HDA) to determine their light absorption characteristics (Figure S3). The wavelength distribution of the absorbed light is an important property of photocatalysts, irrespective of the quantum yield. Therefore, the high photoactivity was attributed to higher visible light absorbance, as indicated by the UV–visible diffuse reflectance spectroscopy. The absorption bands in the range of 200–400 nm, observed in all spectra, suggest strong free exciton absorption at room temperature. The band gap of samples can be estimated from a plot of $(\alpha h\upsilon)^2$ versus the photon energy and the intercept of a tangent to the x-axis was recorded as shown in Figure S4 where energies, Eg, determined from the spectra are 3.28 and 2.28 eV for ZnO(SA) and V_2O_5(HDA) respectively [41]. The variation of the band gap with respect to that of ZnO(SA) is clearly seen, the absorption edge has a clear shift toward longer wavelengths.

In Figure 4a the infrared analysis of ZnO(SA) shows the peaks in the region 3000–2800 cm^{-1} assigned to stretching modes of the C–H bond of the methylene group, the band at 1705 cm^{-1} corroborates the presence of ν(C–O) band of the carboxylic acid in the sample and the bands at 1560 and 1315 cm^{-1} corresponding to the asymmetric and symmetric ν(C–O) modes, respectively, demonstrate that the organic moiety is found as a carboxylate mono-coordinated to the inorganic sheets [42]. In Figure 4b, the infrared analysis of V_2O_5(HDA) shows that the peaks in the region 1000 cm^{-1} are assigned to the stretching vibration of V=O, the frequencies correspond to V=O group of the vanadyl oxygen in 1011, 997 cm^{-1} and V–O–V asymmetric stretching in 737 cm^{-1} of V_2O_5. The stretching modes of the C–H bond of the methylene group at 3000–2800 cm^{-1}. The spectrum shows a shoulder at 3136 cm^{-1} attributed to the N–H vibrational stretching mode of the hexadecylamine surfactant of the nanocomposite [43]. The spectrum infrared the ZnO(SA)/V_2O_5(HDA) composite in Figure 4c shows characteristics bands of both components. The observation in all IR spectra of H–O–H vibrational modes in the region 3500 cm^{-1} indicates a detectable presence of remnant water molecules.

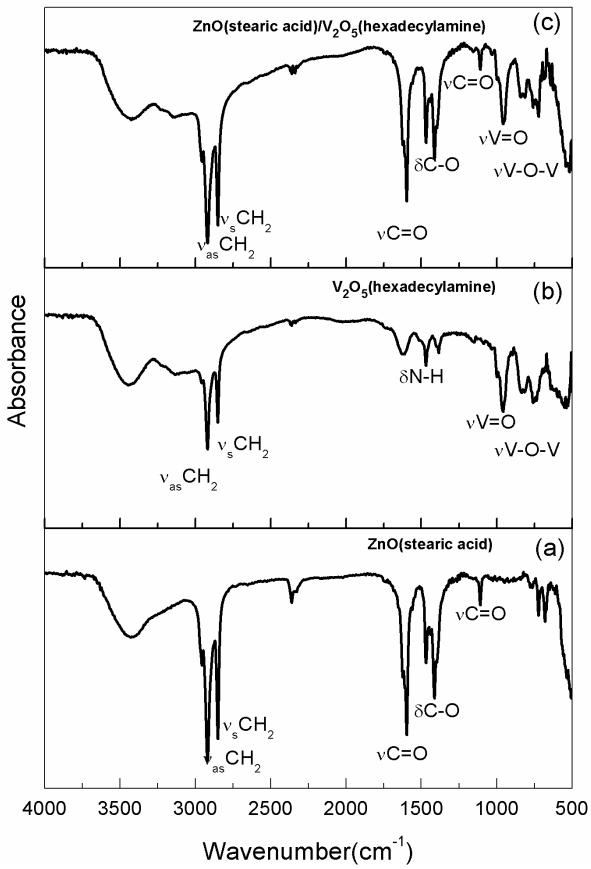

Figure 4. (**a**) FTIR absorbance spectra of ZnO(SA) (**b**) FTIR absorbance spectra of V_2O_5(HDA) and (**c**) FTIR spectra of ZnO(SA)/V_2O_5(HDA).

Photocatalytic Activity

The photocatalytic activity of nanocomposites and their heterojunctures was studied by visible light degradation of methylene blue as a pollutant model. We investigated the photocatalytic behavior a series of samples with different ZnO/V_2O_5 molar ratios prepared by mixing ZnO(SA) and V_2O_5 orthorhombic, V_2O_5-xerogel or V_2O_5(HDA) as described in Table S1. The photocatalytic properties of the as-prepared samples were evaluated under similar conditions and all curves were normalized after reaching the adsorption/desorption equilibrium (Figure S5). The results in Figure 5a shows that the sample of the heterojunction ZnO(SA)/V_2O_5(HDA) 1:0.25 exhibits the highest photocatalytic

efficiency in visible light irradiation. The comparison of catalytic activity of these samples indicated that 90% of the MB dye was degraded after 400 min of irradiation, the luminance of the light source was 0.5 Sun. Meanwhile, the hybrid heterostructure ZnO(SA)/V_2O_5(HDA) 1:0.5 shows lower photocatalytic ability than the other samples, which could be attributed to the higher concentration of V_2O_5 acting as a recombination center for photogenerated charge carriers and increasing the sample opacity, obstructing the light absorption and decreasing the photocatalytic activity [17]. Photocatalytic processes are very complex, and some aspects of the reaction kinetics are being studied. In this work, the photocatalytic degradation of methylene blue could be described by pseudo-first-order kinetics, $\ln(C_0/C) = kt$, where k is the corresponding kinetic constant and t the irradiation time Figure 5b. The apparent rate constants (k_{app}, min^{-1}) hybrid ZnO(SA)/V_2O_5(HDA) was about 6 time faster than for ZnO. The rate constants were calculated and the linear regression coefficients (R^2) for all samples under visible light.

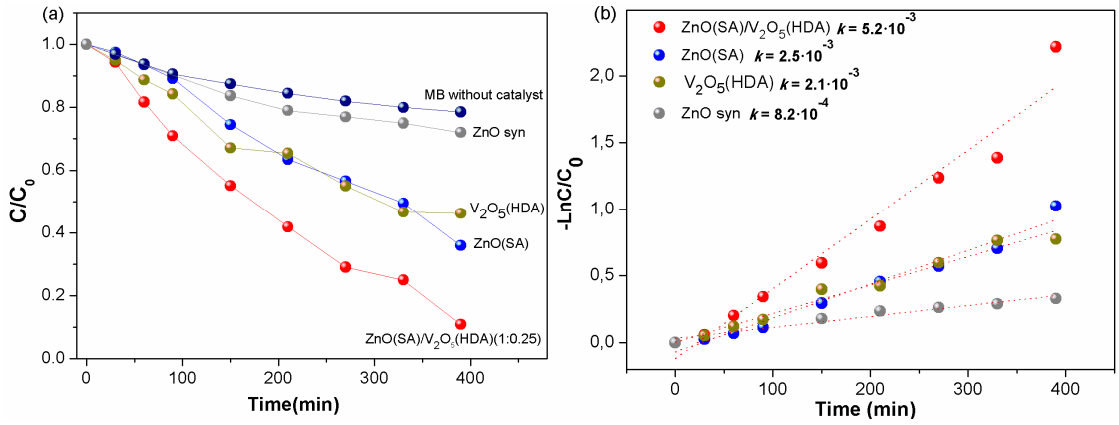

Figure 5. (**a**) Photocatalytic performance of the samples ZnO(SA)/V_2O_5(HDA) for the degradation of MB solution and the degradation of MB without photocatalyst. (**b**) Photodegradation kinetics of the selected samples for the degradation of MB solution.

These results agree qualitatively with reports on the improvement of the photocatalytic efficiency of stratified hybrid ZnO [33,37]. The shape of the MB spectrum remains unchanged throughout the process and no organic by products were detected, indicating the degradation of the dye (Figure S6). The photocatalytic performance of visible light observed indicates that there is a synergistic effect between both 2D nanocomposites used. In these heterojunctions the large face-to-face contact between the sheets, which provide more reaction sites for the adsorption of contaminants exhibiting greater stability, should lead to the interfacial charge transfer efficiency [26,27]. the presence of the organic surfactant in the interlaminar spaces of ZnO and V_2O_5 favors the adsorption of dye on the surface of semiconductors thus the abundance of hydrophobic sites for the adsorption of dye appears as a probable cause of improved photocatalytic efficiency in this hybrid semiconductors heterojunction.

To further investigate the role of active species such as h^+, $^{\bullet}OH$ and $O_2^{-\bullet}$ in the photocatalytic degradation of dye, active species trapping experiments were performed using the sample ZnO(SA), V_2O_5(HDA) and ZnO(SA)/V_2O_5(HDA) 1:0.25. For these experiments, oxalate of ammonium (OA) was used as hole (h^+) scavenger (2 mM), isopropanol (IPA) as a $^{\bullet}OH$ scavenger (2 mM) and chloroform ($CHCl_3$) as an $O_2^{-\bullet}$ scavenger (2 mM) [44–46]. The impact of different scavengers is shown in Figure 6a, for ZnO(SA) (64%), when the $CHCl_3$ was added into reaction solution, the photocatalytic degradation is almost invariable (60%). However, when the IPA and OA were added into solution, the degradation rate of MB was inhibited (44% and 47%, respectively). Thus, the $^{\bullet}OH$ and h^+ radicals are the major reactive species in the ZnO(SA) reaction. For V_2O_5(HDA) (48%), when the IPA was added to the reaction solution photocatalytic degradation drops to 5% indicating that $^{\bullet}OH$ is the major reactive species in the reaction. On the other hand, for the ZnO(SA)/V_2O_5(HDA) sample (90%), when the OA

and IPA were added, the photocatalytic degradation rate was decreased (53% and 54%, respectively) indicating the h^+ and $^{\bullet}OH$ are the predominant active species. When the $CHCl_3$ was added to the reaction solution, the degradation rate of the inhibited slightly (68%), suggesting the $O_2^{-\bullet}$ affects less in the photocatalysis process. Thus, from these experiments, we conclude $^{\bullet}OH$ and h^+ as major active species in photocatalytic degradation of MB under visible light irradiation.

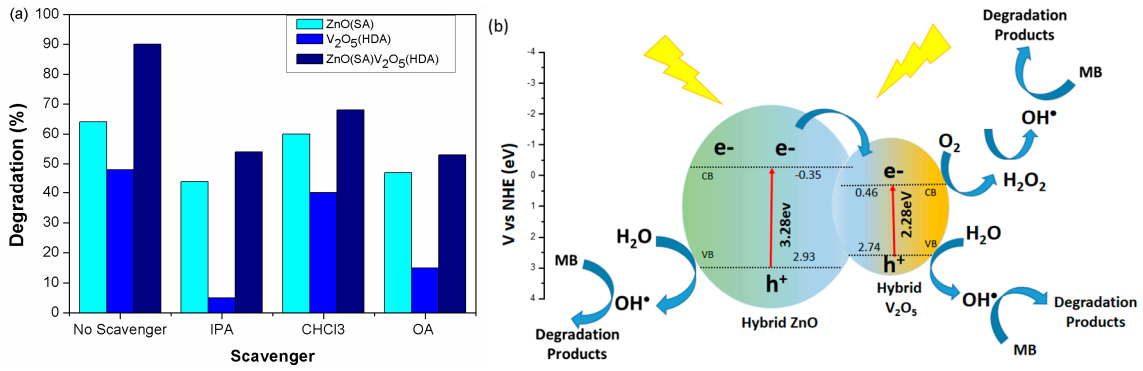

Figure 6. (**a**) Photocatalytic degradation of MB under visible light after addition of several trapping reagents (**b**) Possible mechanism of the photocatalytic activity of $ZnO(SA)/V_2O_5(HDA)$ for degradation under visible light irradiation.

The activity of photocatalyst depends of the effective separation of electron–hole pairs and the migration of the photogenerated charge is related to the band edge position in conduction band (CB) and valence band (VB) of semiconductors. The band positions (E_{CB} and E_{VB}) for the hybrids ZnO and V_2O_5 were calculated applying the equations reported in the literature [46]:

$$E_{CB} = \chi - E^e - \frac{1}{2}E_g$$

$$E_{CB} = E_{VB} - E_g$$

where χ is the electronegativity of semiconductors ZnO and V_2O_5 (5.79 and 6.10 eV, respectively); E^e is the energy of free electrons on the hydrogen scale (4.5 eV); and the band gap energy (E_g) of the semiconductor calculated from DRS data [40]. The calculated CB and VB edge positions of hybrid ZnO are −0.35 eV and 2.93 eV. As for hybrid V_2O_5, the CB and VB edge positions are 0.46 eV and 2.74 eV, respectively.

Therefore, when the photon energy higher or equal to band gap energy of ZnO and V_2O_5, electrons can be excited from the VB to the CB with simultaneous generation of holes in the VB. Due to the CB of ZnO(SA) is more negative than that of the $V_2O_5(HDA)$, electrons on the CB of ZnO(SA) can be easily injected into the CB of $V_2O_5(HDA)$ by the interface. The photogenerated electrons on the CB of $V_2O_5(HDA)$ could not produce $O_2^{-\bullet}$ from dissolved O_2, due to the position of CB is more positive than the potential of $O_2/O_2^{-\bullet}$ (−0.33 V vs. NHE). However, the reduction potential of O_2/H_2O_2 is 0.695 eV vs. NHE, means electrons can react with O_2 and H^+ to produce H_2O_2 which indirectly produce $^{\bullet}OH$ [46]. This is also observed in heterojunctions with other semiconductors like Ag_3VO_4/WO_3 [47], ZnO/MoS_2 [45] and Ag_3PO_4/TiO_2 [48]. Meanwhile the photoinduced holes in VB of both V_2O_5 and ZnO can oxidize adsorbed H_2O molecules to produce $^{\bullet}OH$ ($^{\bullet}OH/H_2O$ is 2.72 eV vs. NHE).

The mechanism can be described as:

$$ZnO(SA)/V_2O_5(HDA) + h\nu\ (visible) \rightarrow ZnO(SA)/V_2O_5(HDA)(h^+\ VB + e^-\ CB)$$

$$ZnO(SA)(e^-\ CB) \rightarrow V_2O_5(HDA)(e^-\ CB)$$

$$ZnO(SA)(h^+\ VB) \rightarrow V_2O_5(HDA)(h^+\ VB)$$

$$V_2O_5(HDA)(e^- CB) + H^+ + O_2 \rightarrow H_2O_2$$

$$H_2O_2 + e^- + h\nu \text{ (visible)} \rightarrow {}^{\bullet}OH + OH^-$$

$${}^{\bullet}OH + h^+ + MB \rightarrow \text{Degradation products}$$

$^{\bullet}$OH radicals are very reactive oxidative species to degrade of dye. As illustrated in Figure 6b, the prepared heterojunctions ZnO/V_2O_5 improve the photogenerated electron–hole pair's separation and transfer, favored by extensive interface area, as well as show an oxidation and reduction ability for efficient degradation of organic pollutants.

Concerning the stability of the photocatalyst, we have also investigated the stability and reusability of the $ZnO(SA)/V_2O_5(HDA)$ photocatalyst over three cycles for a period of 400 min irradiation [46,49]. Figure S7 shows a loss photocatalytic activity of approx. 10% in which might be due to the loss of the photocatalyst by centrifugation, washing and drying of sample, during each cycle of reusability. No significant changes in neither the dye degradation efficiency loss nor photocatalyst structure occur.

3. Materials and Methods

3.1. Materials

All the reagents in this study were commercial products purchased from Sigma-Aldrich (Darmstadt, Germany) and Merck (St. Louis, USA and were used without further purification. Nanopure water was obtained from a water purification system.

3.2. Experimental-Synthesis Nanocomposites

3.2.1. Synthesis of ZnO(Stearic Acid)-ZnO(SA)

ZnO-stearic acid nanocomposite was synthesized as described in a previous paper [36]. In a typical procedure, $ZnSO_4$ (1 mol L^{-1}) was mixed with Na_2CO_3 (1 mol L^{-1})/NaOH (1 mol L^{-1}) (1:1) to bear a ZnO hydrogel; then stearic acid (SA) 4.0×10^{-1} mol L^{-1} aqueous solution was added to the ZnO hydrogel solution under stirring at room temperature; the suspension was stirred at 60 °C followed by an aging period of 24 h at room temperature. The sample was washed and dried at 80 °C for 72 h. Analysis: % found (calculated) for $ZnO(C_{18}H_{36}O_2)_{0.38}\cdot 0.5H_2O$, C: 41.94(41.65), H: 7.20(7.22).

3.2.2. Synthesis of Compounds Vanadium Pentoxide

V_2O_5 xerogel, a mixture of t-butyl alcohol and orthorhombic V_2O_5 was refluxed for 6 h to form the xerogel. Water was added to the resulting dark yellow solid and the remaining t-butyl alcohol was removed with excess water under vacuum. Water was added to yield a suspension. The material was aged at room temperature yielding a red-brown colloidal V_2O_5 [37].

V_2O_5 (hexadecylamine)-V_2O_5(HDA). A solution of 10^{-3} mol of hexadecylamine (HDA) in pure ethanol, previously degassed was mixed with 2×10^{-3} mol of vanadium triisopropoxide (VOTPP) [37]. The yellow solution, obtained after vigorous stirring in an argon atmosphere for 1 h, was then hydrolyzed by adding 15 mL of water. The orange suspension obtained after stirring for 24 h. and subjected to a hydrothermal treatment in a Teflon lined autoclave at 180 °C for 6 days. From the results, an orange solid was separated, washed with pure ethanol and water, the sample was washed and dried at 80 °C for 72 h Analysis: % found (calculated) for $V_2O_5(HDA)_{0.83}\cdot x1.8H_2O$. Anal. C: 38.32(39.06); H: 7.89(8.05); N: 2.79(2.56)

V_2O_5 orthorhombic, Sigma-Aldrich (Darmstadt, Germany)

The samples were mixed mechanically in an agate mortar (relation *w/w*). These samples were denoted as $ZnO(SA)/V_2O_5$; $ZnO(SA)/V_2O_5$-xerogel and $ZnO(SA)/V_2O_5(HDA)$.

3.3. Photocatalytic Experiments

The photocatalytic activity of nanocomposites was studied for the degradation in visible light irradiation of methylene blue as a pollutant model. For this study, the characteristic absorption peak of MB at 664 nm was monitored using a UV-vis spectrophotometer at regular intervals of time and the corresponding absorption spectra. The photocatalytic activity of the products was evaluated by measuring the degradation of methylene blue (MB) in water. The nanocomposite ZnO(SA) (10 mg) and compounds of V_2O_5 in different proportions in 25 mL of a 1×10^{-5} mol L^{-1} which solution phosphate buffer prepared mixing solutions of Na_2HPO_4 and NaH_2PO_4. Prior to irradiation, the suspension was magnetically stirred for 30 min, to establish an adsorption/desorption equilibrium.

The suspensions were irradiated by a 300 W Xe arc lamp (Newport) with a UVIR-CUT filter at $\lambda \geq 400$ nm, the luminance of the light source over the reactant solution was 0.5 Sun. All samples were constant magnetic stirring to ensure a higher level of homogeneity of the photocatalyst in the suspension. The MB concentration after equilibration was regarded as the initial concentration (C_0) and was monitored in the UV-vis spectra of the solution (Perkin Elmer Lambda 35, Shelton, USA), using nanopure water as a reference.

3.4. Characterization

X-ray diffraction (XRD) analyses of the products were performed using a Bruker D8 Advance (Cu Kα λ = 1.5418 Å). The Scanning Electron Microscopy (SEM) and images were obtained by using an EVO MA 10 ZEISS microscope. X-ray photoelectron spectra (XPS) were obtained in a STAIB system with a RQ-300 X-ray source, using monochromated Al Kα X-rays (1486.6 eV, 75 W). The charge referencing was done against adventitious carbon (C 1s 285 eV). Zn 2p, V 2p, O 1s and C1s energy regions were scanned with several sweeps until a good signal-to-noise ratio was observed. Chemical analysis was obtained by using (SISONS ES-1108). The diffuse reflectance UV–vis spectra were recorded in the range of 200–800 nm using a Perkin Elmer Lambda 35 spectrometer. Reflectance measurements were converted to absorption spectra using the Kubelka-Munk function. Fourier transform infrared (FTIR) spectra were recorded an FT/IR-4600 Jasco spectrometer (Tokyo, Japan).

4. Conclusions

In summary, we have reported the successfull fabrication of the new heterojunction of two 2D hybrid semiconductors, ZnO(SA)/V_2O_5(HDA) exhibiting improved photocatalytic activity than the pristine zinc oxide in the degradation of methylene blue under visible light. The efficacy of the products described as catalysts for the photooxidation of organic pollutants is associated with the surface properties of 2D hybrid nanocomposites, collection efficiency for visible light as well as the presence of organic surfactant in the interlaminar spaces of ZnO and V_2O_5 that favors the adsorption of the dye on the surface of semiconductors. The nanocomposites of V_2O_5 effectively inhibit the recombination of photogenerated electron/hole pairs. The products are recyclables and seen as potentially useful for environmental issues remediation.

Supplementary Materials: The following are available online at http://www.mdpi.com/2073-4344/8/9/374/s1, Figure S1. XPS survey spectra; Figure S2. (a) Images SEM of ZnO(SA)/V_2O_5(HDA) (b) Element mappings Zn and V, (c) and (d) Element mappings Zn and V (x5); Figure S3. The UV–visible diffuse reflectance was measured for ZnO(SA),V_2O_5(HDA) and ZnO(SA)/V_2O_5(HDA); Figure S4. Band gap of samples for ZnO(SA) and V_2O_5(HDA); Figure S5. Photocatalytic performance of the samples for the degradation of MB solution; Figure S6. Absorption spectra with time of visible light exposure sample ZnO(SA)/V_2O_5(HDA) (1:0.1); Figure S7. Recycling test of MB photodegradation under visible light of ZnO(SA)/V_2O_5(HDA) (1:0.25) and Table S1. Molar composition of samples prepared and degradation of MB.

Author Contributions: J.A. and N.C. conceived and designed the experiments. N.C. performed the experiments. E.B., C.S.-T. and G.G. analyzed the data and discussed results. J.A. contributed reagents/materials/analysis tools. E.B. and G.G. wrote the paper.

Funding: This research received no external funding.

Acknowledgments: Work supported by UTEM, UCh, FONDECYT 1151189, 1171803, Basal Financing Program CONICYT, FB0807 (CEDENNA). CMST acknowledges the support from the Spanish MINECO projects PHENTOM (FIS2015-70862-P), Severo Ochoa (SEV-2013-0295) and from the CERCA Programme/Generalitat de Catalunya. Conicyt-Programa Fondequip XPS EQM 140044.

Conflicts of Interest: The authors declare no conflict of interest.

References

1. Chan, S.H.; Wu, T.Y.; Juan, J.C.; The, C.Y. Recent developments of metal oxide semiconductors as photocatalysts in advanced oxidation processes (AOPs) for treatment of dye waste-water. *Chem. Technol. Biotechnol.* **2011**, *86*, 1130–1158. [CrossRef]
2. Ray, C.; Pal, T. Recent advances of metal–metal oxide nanocomposites and their tailored nanostructures in numerous catalytic applications. *J. Mater. Chem. A* **2017**, *5*, 9465–9487. [CrossRef]
3. Lang, X.; Chen, X.; Zhao, J. Heterogeneous visible light photocatalysis for selective organic transformations. *Chem. Soc. Rev.* **2014**, *43*, 473–486. [CrossRef] [PubMed]
4. Ibhadon, A.O.; Fitzpatrick, P. Heterogeneous Photocatalysis: Recent Advances and Applications. *Catalysts* **2013**, *3*, 189–219. [CrossRef]
5. Hernandez, S.; Hidalgo, D.; Sacco, A.; Chiodoni, A.; Lamberti, A.; Cauda, V.; Tresso, E.; Saracco, G. Comparison of photocatalytic and transport properties of TiO_2 and ZnO nanostructures for solar-driven water splitting. *Phys. Chem. Chem. Phys.* **2015**, *17*, 7775–7786. [CrossRef] [PubMed]
6. Xia, Y.; Wang, J.; Chen, R.; Zhou, D.; Xiang, L. A Review on the Fabrication of Hierarchical ZnO Nanostructures for Photocatalysis Application. *Crystals* **2016**, *6*, 148. [CrossRef]
7. Banerjee, S.; Dionysiou, D.D.; Pillai, S.C. Self-Cleaning applications of TiO_2 by photo-induced hydrophilicity and photocatalysis. *App. Catal. B Environ.* **2015**, *176–177*, 396–428. [CrossRef]
8. Chen, X.; Wu, Z.; Liu, D.; Gao, Z. Preparation of ZnO photocatalyst for the efficient and rapid photocatalytic degradation of Azo dyes. *Nanoscale Res. Lett.* **2017**, *12*, 143. [CrossRef] [PubMed]
9. Lee, K.M.; Lai, C.W.; Ngai, K.S.; Juan, J.C. Recent developments of zinc oxide based photocatalyst in water treatment technology: A review. *Water Res.* **2016**, *88*, 428–448. [CrossRef] [PubMed]
10. Wang, J.; Xia, Y.; Dong, Y.; Chen, R.; Xiang, L.; Komarneni, S. Defect-rich ZnO nanosheets of high surface area as an efficient visible-light photocatalyst. *App. Catal. B Environ.* **2016**, *192*, 8–16. [CrossRef]
11. Song, X.; Dong, D.; Yang, P. Formation of nanoplate-based clew-like ZnO mesocrystals and their photocatalysis application. *RSC Adv.* **2016**, *6*, 51544–51551. [CrossRef]
12. Fageria, P.; Gangopadhyay, S.; Pande, S. Synthesis of ZnO/Au and ZnO/Ag nanoparticles and their photocatalytic application using UV and visible light. *RSC Adv.* **2014**, *4*, 24962–24972. [CrossRef]
13. Zhang, Y.; Xu, J.; Xu, P.; Zhu, Y.; Chen, X.; Yu, W. Decoration of ZnO nanowires with Pt nanoparticles and their improved gas sensing and photocatalytic performance. *Nanotechnology* **2010**, *21*, 285501–285508. [CrossRef] [PubMed]
14. Mendoza-Mendoza, E.; Nuñez-Briones, A.G.; García-Cerda, L.A.; Peralta-Rodríguez, R.D.; Montes-Luna, A.J. One-step synthesis of ZnO and Ag/ZnO heterostructures and their photocatalytic activity. *Ceram. Int.* **2018**, *44*, 6176–6180. [CrossRef]
15. Mani, J.; Sakeek, H.; Habouti, S.; Dietze, M.; Es-Souni, M. Macro–meso-porous TiO_2, ZnO and ZnO-TiO_2 composite thick films. Properties and application to photocatalysis. *Catal. Sci. Technol.* **2012**, *2*, 379–385. [CrossRef]
16. Balachandran, S.; Prakash, N.; Thirumalai, K.; Muruganandham, M.; Sillanpää, M.; Swaminathan, M. Facile construction of heterostructured $BiVO_4$–ZnO and its dual application of greater solar photocatalytic activity and self-cleaning property. *Ind. Eng. Chem. Res.* **2014**, *53*, 8346–8356. [CrossRef]
17. Sun, C.; Fu, Y.; Wang, Q.; Xing, L.; Liu, B.; Xue, X. Ultrafast piezo-photocatalytic degradation of organic pollutions by Ag_2O/tetrapod-ZnO nanostructures under ultrasonic/UV exposure. *RSC Adv.* **2016**, *6*, 87446–87453. [CrossRef]
18. Kandjani, K.; Sabri, Y.; Periasamy, S.; Zohora, N.; Amin, M.; Nafady, A.; Bhargava, S. Controlling core/shell formation of nanocubic p-Cu_2O/n-ZnO toward enhanced photocatalytic performance. *Langmuir* **2015**, *39*, 10922–10930. [CrossRef] [PubMed]

19. Vikas, L.S.; Vanaja, K.A.; Subha, P.P.; Jayaraj, M.K. Fast UV sensing properties of n-ZnO nanorods/p-GaN heterojunction. *Sens. Actuators A* **2016**, *242*, 116–122. [CrossRef]
20. Adhikari, S.; Sarkar, D.; Madras, G. Highly efficient WO_3–ZnO mixed oxides for photocatalysis. *RSC Adv.* **2015**, *5*, 11895–11904. [CrossRef]
21. Ahmeda, L.T.; Ma, M.; Edvinsson, T.; Zhua, J. A facile approach to ZnO/CdS nanoarrays and their photocatalytic and photoelectrochemical properties. *App. Catal. B Environ.* **2013**, *138–139*, 175–183.
22. Zaera, F. New challenges in heterogeneous catalysis for the 21st century. *Catal. Lett.* **2012**, *142*, 501–516. [CrossRef]
23. Ebrahimi, M.; Samadi, M.; Yousefzadeh, S.; Soltani, M.; Rahimi, A.; Chou, T.; Chen, L.; Chen, K.; Moshfegh, A. Improved solar-driven photocatalytic activity of hybrid graphene quantum dots/ZnO nanowires: A direct Z-scheme mechanism. *ACS Sustain. Chem. Eng.* **2017**, *5*, 367–375. [CrossRef]
24. Colombo, E.; Li, W.; Bhangu, S.; Ashokkumar, M. Chitosan microspheres as a template for TiO_2 and ZnO microparticles: Studies on mechanism, functionalization and applications in photocatalysis and H_2S removal. *RSC Adv.* **2017**, *7*, 19373–19383. [CrossRef]
25. Anastasio, P.; Del Giacco, T.; Germani, R.; Spretic, N.; Tiecco, M. Structure effects of amphiphilic and non-amphiphilic quaternary ammonium salts on photodegradation of Alizarin Red-S catalysed by titanium dioxide. *RSC Adv.* **2017**, *7*, 361–368. [CrossRef]
26. Low, J.; Cao, S.; Yu, J.; Wageh, S. Two-dimensional layered composite photocatalysts. *Chem. Commun.* **2014**, *50*, 10768–10777. [CrossRef] [PubMed]
27. Li, Y.; Li, Y.L.; Sa, B.; Ahujad, R. Review of two-dimensional materials for photocatalytic water splitting from a theoretical perspective. *Catal. Sci. Technol.* **2017**, *7*, 545–559. [CrossRef]
28. Zhang, Z.; Huang, J.; Zhang, M.; Yuan, Q.; Dong, B. Ultrathin hexagonal SnS2 nanosheets coupled with g-C_3N_4 nanosheets as 2D/2D heterojunction photocatalysts toward high photocatalytic activity. *Appl. Catal. B* **2015**, *163*, 298–305. [CrossRef]
29. Yuan, C.; Hung, C.; Yuan, C.; Wen, H. Preparation and application of immobilized surfactant-modified PANi-CNT/TiO_2 under visible-light irradiation. *Materials* **2017**, *10*, 877. [CrossRef] [PubMed]
30. Zhu, X.; Yuan, C.; Chen, C. Photocatalytic degradation of pesticide pyridaben. 3. In surfactant/TiO_2 aqueous dispersions. *Environ. Sci. Technol.* **2007**, *41*, 263–269. [CrossRef] [PubMed]
31. Duta, M.; Perniu, D.; Duta, A. Photocatalytic zinc oxide thin films obtained by surfactant assisted spray pyrolysis deposition. *App. Surf. Sci.* **2014**, *306*, 80–88. [CrossRef]
32. Hao, C.; Wang, J.; Cheng, Q.; Bai, Y.; Wang, X.; Yang, Y. Anionic surfactants-assisted solution-phase synthesis of ZnO with improved photocatalytic performance. *J. Photochem. Photobiol. A Chem.* **2017**, *332*, 384–390. [CrossRef]
33. Benavente, E.; Navas, D.; Devis, S.; Segovia, M.; Sotomayor-Torres, C.; González, G. Composites of laminar nanostructured ZnO and VOx-Nanotubes hybrid as visible light active photocatalysts. *Catalysts* **2018**, *8*, 93. [CrossRef]
34. Yin, H.; Yu, K.; Hu, J.; Song, C.; Guo, B.; Wang, Z.; Zhu, Z. Novel photoluminescence properties and enhanced photocatalytic activities for V_2O_5-loaded ZnO nanorods. *Dalton Trans.* **2015**, *10*, 4671–4678. [CrossRef] [PubMed]
35. Zou, C.W.; Rao, Y.F.; Alyamani, A.; Chu, W.; Chen, M.J.; Patterson, D.A.; Emanuelsson, E.A.; Gao, W. Heterogeneous lollipop-like V_2O_5/ZnO Array: A promising composite nanostructure for visible light photocatalysis. *Langmuir* **2010**, *14*, 11615–11620. [CrossRef] [PubMed]
36. Aslam, M.; Ismail, I.; Almeelbi, T.; Salah, N.; Chandrasekaran, S.; Hameed, A. Enhanced photocatalytic activity of V_2O_5–ZnO composites for the mineralization of nitrophenols. *Chemosphere* **2014**, *117*, 115–123. [CrossRef] [PubMed]
37. Segovia, M.; Lemus, K.; Moreno, M.; Santa Ana, M.A.; González, G.; Ballesteros, B.; Sotomayor, C.; Benavente, E. Zinc oxide/carboxylic acid lamellar structures. *Mater. Res. Bull.* **2011**, *46*, 2191–2195. [CrossRef]
38. O'Dwyer, C.; Navas, D.; Lavayen, V.; Benavente, E.; Santa Ana, M.A.; González, G.; Newcomb, S.B.; Sotomayor Torres, C.M. Nano-Urchin: The formation and structure of high-density spherical clusters of vanadium oxide nanotubes. *Chem. Mater.* **2006**, *13*, 3016–3022. [CrossRef]
39. Asim, N.; Radiman, S.; Yarmo, M.A. Preparation and characterization of core–shell polyaniline/V_2O_5 nanocomposite via microemulsion method. *Mater. Lett.* **2008**, *62*, 1044–1047. [CrossRef]

40. Martha, S.; Das, D.P.; Biswal, N.; Parida, K.M. Facile synthesis of visible light responsive V_2O_5/N,S–TiO_2 composite photocatalyst: Enhanced hydrogen production and phenol degradation. *J. Mater. Chem.* **2012**, *22*, 10695–10703. [CrossRef]
41. Xu, Y.; Schoonen, M. The absolute energy positions of conduction and valence bands of selected semiconducting minerals. *Am. Mineral.* **2000**, *85*, 543–556. [CrossRef]
42. Mendive, C.B.; Bahnemann, D.W.; Blesa, M.A. Microscopic characterization of the photocatalytic oxidation of oxalic acid adsorbed onto TiO_2 by FTIR-ATR. *Catal. Today* **2005**, *101*, 237–244. [CrossRef]
43. O'Dwyer, C.; Lavayen, V.; Newcomb, S.B.; Santa Ana, M.A.; Benavente, E.; González, G.; Sotomayor-Torres, C.M. Vanadate conformation variations in vanadium pentoxide nanostructures. *J. Electrochem. Soc.* **2007**, *154*, K29–K35. [CrossRef]
44. Liu, H.R.; Shao, G.X.; Zhao, J.F.; Zhang, Z.X.; Zhang, Y.; Liang, J.; Liu, X.G.; Jia, H.S.; Xu, B.S. Worm-like Ag/ZnO core-shell heterostructural composites: Fabrication, characterization, and photocatalysis. *J. Phys. Chem. C* **2012**, *116*, 16182–16190. [CrossRef]
45. Kumar, S.; Sharma, V.; Bhattacharyya, K.; Krishnana, V. N-doped ZnO-MoS_2 binary heterojunctions: Dual role of 2D MoS2 in the enhancement of photostability and photocatalytic activity under visible light irradiation for tetracycline degradation. *Mater. Chem. Front.* **2017**, *1*, 1093–1106. [CrossRef]
46. Hong, Y.; Jiang, Y.; Li, C.; Fan, W.; Yan, X.; Yan, M.; Shi, W. In-situ synthesis of direct solid-state Z-scheme V_2O_5/g-C_3N_4 heterojunctions with enhanced visible light efficiency in photocatalytic degradation of pollutants. *Appl. Catal. B.* **2016**, *180*, 663–673. [CrossRef]
47. Yan, M.; Wu, Y.; Zhu, F.; Hua, Y.; Shi, W. The fabrication of a novel Ag_3VO_4/WO_3 heterojunction with enhanced visible light efficiency in the photocatalytic degradation of TC. *Phys. Chem. Chem. Phys.* **2016**, *18*, 3308–3315. [CrossRef] [PubMed]
48. Tong, Z.H.; Yang, D.; Sun, Y.Y.; Tian, Y.; Jiang, Z.Y. In situ fabrication of Ag_3PO_4/TiO_2 nanotube heterojunctions with enhanced visible-light photocatalytic activity. *Phys. Chem. Chem. Phys.* **2015**, *17*, 12199–12206. [CrossRef] [PubMed]
49. Dong, F.; Sun, Y.; Fu, M. Enhanced visible light photocatalytic activity of V_2O_5 cluster modified N-Doped TiO_2 for degradation of toluene in air. *Int. J. Photoenergy* **2012**, *10*, 569716.

© 2018 by the authors. Licensee MDPI, Basel, Switzerland. This article is an open access article distributed under the terms and conditions of the Creative Commons Attribution (CC BY) license (http://creativecommons.org/licenses/by/4.0/).